

# Relativistic kinetic approach to light nuclei production in high-energy nuclear collisions

Kai-Jia Sun,<sup>1,\*</sup> Rui Wang,<sup>2,3,†</sup> Che Ming Ko,<sup>1,‡</sup> Yu-Gang Ma,<sup>2,3,§</sup> and Chun Shen<sup>4,5,¶</sup>

<sup>1</sup>*Cyclotron Institute and Department of Physics and Astronomy,  
Texas A&M University, College Station, Texas 77843, USA*

<sup>2</sup>*Key Laboratory of Nuclear Physics and Ion-beam Application (MOE),  
Institute of Modern Physics, Fudan University, Shanghai 200433, China*

<sup>3</sup>*Shanghai Institute of Applied Physics, Chinese Academy of Sciences, Shanghai 201800, China*

<sup>4</sup>*Department of Physics and Astronomy, Wayne State University, Detroit, MI 48201, USA*

<sup>5</sup>*RIKEN BNL Research Center, Brookhaven National Laboratory, Upton, NY 11973, USA*

(Dated: June 25, 2021)

Understanding the production mechanism of light (anti-)nuclei in high-energy nuclear collisions and cosmic rays has been a long-standing problem in nuclear physics. In the present study, we develop a stochastic method to solve the relativistic kinetic equations for light nuclei production from many-body reactions with the inclusion of their finite sizes. The present approach gives an excellent description of the deuteron and helium-3 data from central Au+Au (Pb+Pb) collisions at  $\sqrt{s_{NN}} = 200$  GeV (2.76 TeV). It can also naturally explain their suppressed production in  $pp$  collisions at 7 TeV as a result of their finite sizes.

## I. INTRODUCTION

Besides ordinary hadrons in the Standard Model, light nuclei, such as deuteron ( $d$ ), helium-3 ( ${}^3\text{He}$ ), triton ( $t$ ), helium-4 ( ${}^4\text{He}$ ), hypertriton ( ${}^3_{\Lambda}\text{H}$ ) and their antiparticles, have also been observed in high energy nucleus-nucleus ( $AA$ ), proton-nucleus ( $pA$ ), and  $pp$  collisions at the Relativistic Heavy Ion Collider (RHIC) and the Large Hadron Collider (LHC) [1–3]. Although rarely produced, these weakly bound nuclei carry important information on the space-time geometry [4], entropy production [5], and the QCD phase transitions [6–9] in these collisions. They can also provide indirect information on the dark matter interaction in cosmic rays due to their ultra-low astrophysical background [10–12].

Different mechanisms have been proposed to describe light nuclei production in nuclear reactions. For heavy-ion collisions at high energies, the created fireball evolves through stages of pre-equilibrium, the Quark-Gluon Plasma (QGP) or partonic expansion, the hadronization, and subsequent hadronic scatterings and decays until kinetic freeze-out. In the statistical hadronization model [13], light nuclei are thermally produced during the hadronization of QGP and their yields are assumed to remain unchanged during the hadronic evolution. In the coalescence model [14, 15], light nuclei are produced from nucleons close in phase space at the kinetic freeze-out. Since the cross section for the deuteron dissociation by pion reaction  $\pi d \rightarrow \pi NN$  is about 100 mb [16], the rate for the inverse process  $\pi NN \rightarrow \pi d$  in hadronic matter is

also large due to the time-reversal symmetry. Therefore, to understand light nuclei production in high-energy nuclear collisions, it is essential to include their formation and dissociation dynamics in these collisions. The process  $\pi d \leftrightarrow \pi NN$  has recently been studied in Ref. [17] by approximating it as two-step processes of  $NN \leftrightarrow d'$  and  $\pi d' \leftrightarrow \pi d$  with  $d'$  being a fictitious dibaryon resonance. For nuclear reactions at low energies, the process  $NNN \leftrightarrow Nd$  is more important because the produced matter consists mainly of baryons [18]. In all previous transport model studies [17–20], light nuclei have been considered as point particles. This is a valid assumption in large collision systems, but no longer holds in small systems like  $pp$  collisions, in which the size of produced matter is comparable to or even smaller than those of light nuclei such as the  $d$  and  ${}^3_{\Lambda}\text{H}$  [21, 22]. Other proposed mechanisms for light nuclei production in high-energy nuclear collisions include the decay of a compact quark droplet [23] or pre-formed nuclear clusters [24]. In spite of these efforts, the production mechanism of light (anti-)(hyper-)nuclei in nuclear collisions has not yet been unambiguously understood [25–27].

In the present article, we study the dynamics of light nuclei in nuclear collisions by the relativistic kinetic equations that were derived from the time evolution of the system's Green's functions defined on a closed path in time [18, 28–30]. In this approach, the effect of finite sizes of light nuclei, which is usually neglected, can be included by retaining the relative coordinates between nucleons in the gradient expansion of the Green's function [28, 29]. A central quantity in the relativistic kinetic equations is the many-body transition matrix for light nuclei production and dissociation, which will be evaluated here by using the impulse approximation. To illustrate the validity of the impulse approximation, we take  $\pi d \rightarrow \pi NN$  as an example. Since the typical temperature of the hadronic matter in high-energy nuclear collisions is 100-150 MeV, the pion thermal wavelength

\* kjsun@tamu.edu

† wangrui@sinap.ac.cn;

Kai-Jia Sun and Rui Wang contributed equally to this work.

‡ ko@comp.tamu.edu

§ mayugang@fudan.edu.cn

¶ chunshen@wayne.edu

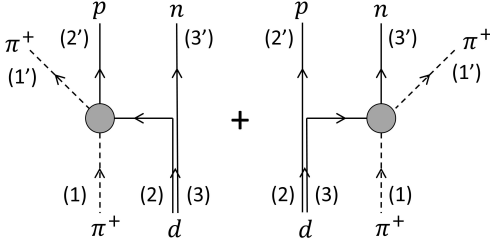


FIG. 1. Diagrams for the reaction  $\pi^+d \leftrightarrow \pi^+np$  in the impulse approximation. Inside the bubble is a  $\Delta$  resonance as an intermediate state.

is then around 0.4-0.5 fm and is much smaller than the deuteron size of about 3 fm. A pion thus has a sufficiently large momentum to resolve the two constituent nucleons in the deuteron, resulting its scattering by one nucleon with the other nucleon being quasifree, as shown in Fig. 1. Therefore, the transition amplitude  $\mathcal{M}_{\pi d \rightarrow \pi NN}$  for this reaction can be approximately factorized and is proportional to  $\langle \tilde{p}_N | \phi_d \rangle \mathcal{M}_{\pi N \rightarrow \pi N}$ , with  $\langle \tilde{p}_N | \phi_d \rangle$  and  $\mathcal{M}_{\pi N \rightarrow \pi N}$  being the deuteron wave function and the  $\pi$ - $N$  elastic scattering amplitude, respectively. The impulse or quasifree approximation was previously used in studying deuteron dissociation in low-energy heavy-ion collisions [18, 31] and also  $J/\Psi$  dissociation by partons in relativistic heavy-ion collisions [32]. Under this approximation, the inverse reaction  $\pi NN \rightarrow \pi d$  can be viewed as a superposition of two subprocesses, the scattering between a pion and a nucleon with the final-state nucleon slightly off mass shell, and followed by the fusion or coalescence of the off-shell nucleon and another nucleon to form a deuteron. The impulse approximation can be generalized straightforwardly to study the production and dissociation of heavier nuclei that involve more than two nucleons.

## II. RELATIVISTIC KINETIC EQUATION

We start by considering one specific channel  $\pi^+d \leftrightarrow \pi^+np$ . Its effect on deuteron production and dissociation in nuclear collisions can be described by the relativistic kinetic equation [18, 29],

$$\frac{\partial f_d}{\partial t_d} + \frac{\mathbf{P}}{E_d} \cdot \frac{\partial f_d}{\partial \mathbf{R}} = -\mathcal{K}^> f_d + \mathcal{K}^< (1 + f_d). \quad (1)$$

where the deuteron distribution function  $f_d(\mathbf{R}, \mathbf{P})$  is normalized as  $g_d(2\pi)^{-3} \int d^3\mathbf{R} d^3\mathbf{P} f_d = N_d$  with  $g_d = 3$  and  $N_d$  being the deuteron statistical spin factor and total yield, respectively.

On the l.h.s. of Eq. (1), which denotes the drift term, we have treated deuteron as a free particle by neglecting its interaction with medium. The two terms on the r.h.s. of Eq. (1) describes the deuteron dissociation and production rates, respectively. Under the impulse approxi-

mation, the collision integral on r.h.s. is given by [18, 30]

$$\begin{aligned} & \frac{1}{2g_d E_d} \int \prod_{i=1',3'} \frac{d^3 \mathbf{p}_i}{(2\pi)^3 2E_i} \frac{d^3 \mathbf{p}_\pi}{(2\pi)^3 2E_\pi} \frac{E_d d^3 \mathbf{r}}{m_d} \\ & \times 2m_d W_d(\tilde{\mathbf{r}}, \tilde{\mathbf{p}}) (|\mathcal{M}_{\pi^+n \rightarrow \pi^+n}|^2 + n \leftrightarrow p) \\ & \times \left[ - \left( \prod_{i=1'}^{3'} (1 \pm f_i) \right) g_\pi f_\pi g_d f_d + \frac{3}{4} \left( \prod_{i=1'}^{3'} g_i f_i \right) \right. \\ & \left. \times (1 + f_\pi)(1 + f_d) \right] \times (2\pi)^4 \delta^4(p_{\text{in}} - p_{\text{out}}), \quad (2) \end{aligned}$$

from which  $\mathcal{K}^>$  and  $\mathcal{K}^<$  in Eq. (1) can be identified. In the above equation, the  $1 \pm f_i$  in the square bracket come from the quantum statistics of fermions ( $-$ ) and bosons ( $+$ ), and the  $\delta$ -function denotes the conservation of energy and momentum with  $p_{\text{in}} = \sum_{i=1'}^{3'} p_i$  and  $p_{\text{out}} = p_\pi + p_d$ . The factor  $3/4$  in the third line comes from the spin factors of initial and final states. The second line of Eq. (2) denotes the spin-averaged squared amplitude at a relative distance  $\mathbf{r}$  between the two nucleons. The  $W_d$  denotes the deuteron Wigner function, with  $\tilde{\mathbf{r}} = \tilde{\mathbf{r}}_n - \tilde{\mathbf{r}}_p$  and  $\tilde{\mathbf{p}} = (\tilde{\mathbf{p}}_n - \tilde{\mathbf{p}}_p)/2$  being the relative coordinate and momentum in deuteron center-of-mass frame, respectively. For simplicity, we take  $W_d = 8e^{-\tilde{r}^2/\sigma_d^2 - \tilde{p}^2\sigma_d^2}$  with  $\sigma_d = 3.2$  fm to reproduce the deuteron root-mean-square radius of 1.96 fm [14].

For an approximately uniform system, the spatial part of  $W_d$  in Eq. (2) can be integrated out, i.e.,  $|\phi_d(\tilde{\mathbf{p}})|^2 = \int d^3\mathbf{r} \gamma_d W_d = (4\pi\sigma_d^2)^{3/2} e^{-\tilde{p}^2\sigma_d^2}$  with  $\gamma_d = E_d/m_d$ , simplifying the second line of Eq. (2) to  $2m_d |\phi_d|^2 (|\mathcal{M}_{\pi^+n \rightarrow \pi^+n}|^2 + n \rightarrow p)$ , which is the usual impulse approximation for  $|\mathcal{M}_{\pi^+d \rightarrow \pi^+np}|^2$ , e.g. adopted in Ref. [18] by treating deuteron as a point particle.

The spin averaged squared pion-nucleon scattering matrix element  $|\mathcal{M}_{\pi^+n \rightarrow \pi^+n}|^2$  can be related to the  $\pi N$  scattering cross section. Under the impulse approximation, the deuteron dissociation cross section by a pion of momentum  $p_{\text{lab}}$  is approximately given by  $\sigma_{\pi^+d \rightarrow \pi^+np} \approx \sigma_{\pi^+n \rightarrow \pi^+n} + \sigma_{\pi^+p \rightarrow \pi^+p}$ . This relation becomes exact only for extremely large  $p_{\text{lab}}$  [16, 18]. At low  $p_{\text{lab}}$ , e.g. 0.3 GeV, one can introduce a renormalization factor  $F_d$  [18] such that  $\sigma_{\pi^+d \rightarrow \pi^+np} = F_d(\sigma_{\pi^+n \rightarrow \pi^+n} + \sigma_{\pi^+p \rightarrow \pi^+p})$ . As shown in Fig. 2, using the constant values  $F_d \approx 0.72$  and  $F_{3\text{He}} \approx 0.51$  leads to an excellent description of the data for the  $\pi + d$  and  $\pi + {}^3\text{He}$  cross sections in the energy region relevant for present study.

Given the above deuteron dissociation and production cross sections with a pion, the probability for the reaction  $\pi^+d \rightarrow \pi^+np$  between a pion and a deuteron inside a volume  $\Delta V$  to take place within a time interval  $\Delta t$  can be obtained as

$$P_{23}|_{\text{IA}} \approx F_d v_{12} \sigma_{\pi^+p \rightarrow \pi^+p} \frac{\Delta t}{\Delta V} + (2 \leftrightarrow 3), \quad (3)$$

where  $v_{12}$  is the relative velocity between the pion and one of the two nucleons inside deuteron, and the two terms on r.h.s correspond to the two diagrams in Fig. 1.

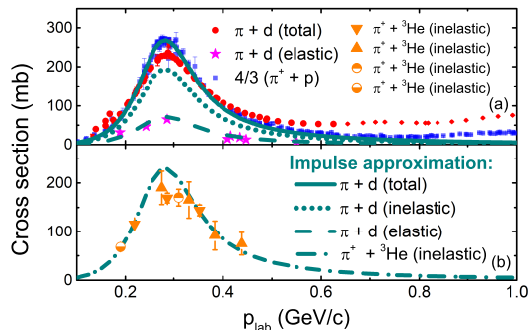


FIG. 2. Comparison of the pion incident momentum ( $p_{\text{lab}}$ ) dependence of the cross sections for the reactions  $\pi + d$  (upper panel) and  $\pi + {}^3\text{He}$  (lower panel) between experimental data [16, 33–38] and our theoretical fit based on the impulsive approximation (colored lines).

Similarly, the probability for the reaction  $\pi^+ np \rightarrow \pi^+ d$  is

$$P_{32}|_{\text{IA}} \approx \frac{3}{4} F_d v_{1'2'} \sigma_{\pi^+ p \rightarrow \pi^+ p} \frac{\Delta t}{\Delta V} W_d + (2' \leftrightarrow 3'). \quad (4)$$

In obtaining Eqs. (3) and (4), we have neglected the factors  $1 \pm f_i$  in Eq. (2), which is a good approximation in high-energy nuclear collisions. Note that the deuteron Wigner function  $W_d$  in Eq. (4) depends on both the coordinates and momenta of the constituent nucleons. It should be replaced by  $|\phi_d|^2/(\gamma_d \Delta V)$  if the deuteron is treated as a point particle.

In the limit that the production and dissociation rates are equal in Eq. (2), one obtains the equilibrated deuteron abundance as

$$N_d \approx \frac{3}{4} \int d\Gamma_{np} g_n f_n(\mathbf{r}_n, \mathbf{p}_n^*) g_p f_p(\mathbf{r}_p, \mathbf{p}_p) W_d(\tilde{\mathbf{r}}, \tilde{\mathbf{p}}), \quad (5)$$

where  $d\Gamma_{np} = (2\pi)^{-6} d^3\mathbf{r}_n d^3\mathbf{p}_n d^3\mathbf{r}_p d^3\mathbf{p}_p$  and the neutron is chosen to be off mass shell to conserve energy [14]. The equilibrium solution given by Eq. (5) is similar to the result from the phase-space coalescence model based on the sudden approximation [39]. Note that the two nucleons in Eq. (5) can be  $nn$ ,  $np$ , or  $pp$  pair, while only the  $np$  pair is considered in the coalescence model. For a uniform and thermalized system, Eq. (5) can be further simplified to  $N_d \approx g_d V (2\pi)^{-3} \int d^3\mathbf{p}_d f_n(\frac{\mathbf{p}_d}{2}) f_p(\frac{\mathbf{p}_d}{2})$ , which is the same as the deuteron abundance in chemical equilibrium with nucleons, indicating that our approach has the correct thermal limit.

### III. NUMERICAL IMPLEMENTATION AND VALIDATION

To solve Eq. (1) with the collision integral given by Eq. (2), we adopt the test particle ansatz [40] (or the particle in cell method), i.e., mimicking the distribution function  $f_\alpha$  of a certain particle species of number  $N_\alpha$  by a large number of delta functions,  $f_\alpha(\mathbf{r}, \mathbf{p})$

$\approx \sum_{i=1}^{N_\alpha N_{\text{test}}} \delta(\mathbf{r}_i - \mathbf{r}) \delta(\mathbf{p}_i - \mathbf{p})$ . Using test particles modifies Eq. (3) and Eq. (4) by the multiplication of factors  $1/N_{\text{test}}$  and  $1/N_{\text{test}}^2$ , respectively. The number of test particles  $N_{\text{test}}$  should be sufficiently large to ensure the convergence of the numerical results. To illustrate the numerical algorithm used in the present study, we take the reaction  $\pi d \rightarrow \pi NN$  as an example. In each time step  $\Delta t$ , a (test) pion and a (test) deuteron are randomly chosen from a cell of volume  $\Delta V$ , and the momenta of two nucleons inside the deuteron is then sampled according to its wave function with one nucleon slightly off mass shell to conserve energy and momentum. After the scattering of the pion with the off-shell nucleon, both final state nucleon and pion are taken to be on mass shell. A similar consideration applies to the inverse reaction  $\pi NN \rightarrow \pi d$ . One first randomly chooses a (test) pion and a (test) nucleon during a time step  $\Delta t$  from a cell of volume  $\Delta V$ . After letting the pion to scatter with the nucleon, their final momenta are then sampled according to the differential cross section but with the nucleon to be off-shell, which subsequently coalesces with the other nearby nucleon to form a deuteron. Since we employ the stochastic method [18, 41, 42], the probabilities of these two processes are directly evaluated according to Eq. (3) and Eq. (4), respectively.

As for triton, it can be formed from the two reactions  $\pi NNN \leftrightarrow \pi t$  and  $\pi dN \leftrightarrow \pi t$ . The  $3 \leftrightarrow 2$  process can be similarly treated as for deuteron production. The probability of the  $4 \leftrightarrow 2$  process to occur in a volume  $\Delta V$  during a time step  $\Delta t$  is given by

$$P_{42}|_{\text{IA}} \approx \frac{1}{4} F_t \frac{v_{\pi N} \sigma_{\pi N \rightarrow \pi N} \Delta t}{N_{\text{test}}^3 \Delta V} W_t, \quad (6)$$

where  $F_t \approx F_{3\text{He}} \approx 0.51$  and the  $W_t$  is the triton Wigner function, and its expression can be found in Refs. [14, 43]. The branching ratio for the dissociation of triton via the two inverse reactions can be estimated by calculating the deuteron component in the triton wave function. If we take the wave function to have the Gaussian form, we have the branching ratio  $\mathcal{B}(\pi t \rightarrow \pi Nd) \approx 0.56$ . More realistic Hulthen wave function for the deuteron leads to a similar branching ratio  $\mathcal{B}(\pi t \rightarrow \pi Nd) \approx 0.58$ . Similarly, the branching ratio for  ${}^3\text{He}$  dissociation to a deuteron is  $\mathcal{B}(\pi {}^3\text{He} \rightarrow \pi Nd) \approx 0.6$ . We note the following numerical results are insensitive to the value of the branching ratios in the production and dissociation of triton and helium-3.

To validate the above described algorithm, we consider deuteron and triton production from a hadronic matter in a  $(20 \text{ fm})^3$  box with periodic boundary conditions. The box consists of 24 protons, 24 neutrons, and 480 pions for each of its three charge states. The initial distribution of these particles is taken to be uniform in the coordinate space and to have a thermal Boltzmann distribution with temperature  $T = 155 \text{ MeV}$  in the momentum space. Fig. 3 (a) shows the time evolution of the yields of proton, deuteron, and triton (helium-3). It is seen that their final numbers are consistent with their thermal values at chemical equilibrium over 5 orders of magnitude.

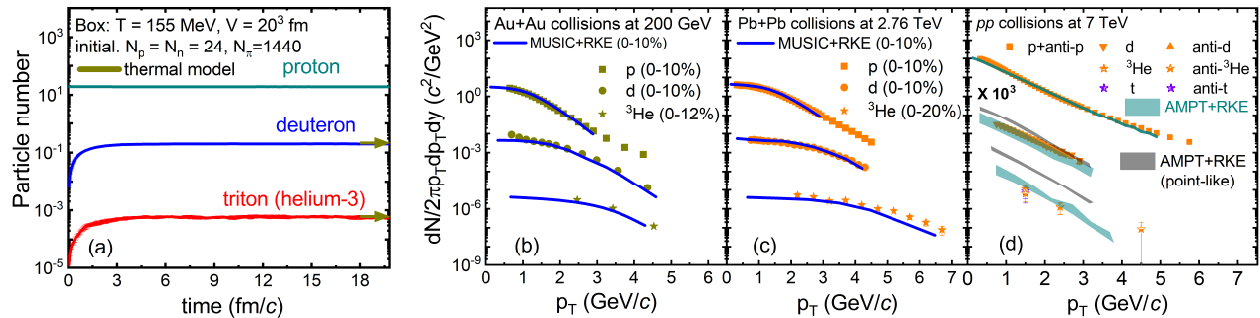


FIG. 3. Panel (a) Box calculations for deuteron and triton (helium-3). Transverse momentum spectra of  $p$ ,  $d$ , and  ${}^3\text{He}$  ( $t$ ) in (b) central Au+Au collisions at  $\sqrt{s_{\text{NN}}} = 200$  GeV; (c) central Pb+Pb collisions at  $\sqrt{s_{\text{NN}}} = 2.76$  TeV; (d)  $pp$  collisions at  $\sqrt{s_{\text{NN}}} = 7$  TeV. The experimental data points are taken from Refs. [44–50]. Theoretical predictions from the relativistic kinetic equations (RKE) are denoted by colored lines. The spectra in panel (d) are multiplied by a factor of  $10^3$ .

#### IV. LIGHT NUCLEI PRODUCTION IN HIGH-ENERGY NUCLEAR COLLISIONS

We now apply the above described kinetic approach to different collision systems, i.e., central Au+Au collisions at  $\sqrt{s_{\text{NN}}} = 200$  GeV, Pb+Pb collisions at  $\sqrt{s_{\text{NN}}} = 2.76$  TeV, and  $pp$  collisions at 7 TeV. For the evolution of the QGP produced in central Au+Au and Pb+Pb collisions, we use the (3+1)-d viscous hydrodynamic model MUSIC [51–54] with initial conditions taken from a newly developed dynamical Glauber model [52, 55]. The QGP has a smooth crossover to a hadronic matter along a phase transition line  $T(\mu_B)$  described in Ref. [56]. The initial hadrons are sampled on a constant energy density particalization hypersurface according to the Cooper-Frye formula [57]. For  $pp$  collisions, the initial hadron distribution is generated from a multiphase transport (AMPT) model [58]. In the present article, we also assume that light nuclei are initially produced from hadronization of QGP, and their yields are estimated from the canonical statistical model [59] that conserves baryon, electric and strange charges.

For the evolution of the hadronic matter and the production of light nuclei, besides the production and dissociation of deuteron and helium-3 by pions, most scattering channels in AMPT [58] have been included. These channels describe properly the dynamics of pions and nucleons that are relevant for light nuclei production from the reactions discussed above.

Fig. 3 (b) and (c) show the comparison of the transverse momentum ( $p_T$ ) spectra of  $p$ ,  $d$ , and  ${}^3\text{He}$  between our predictions and the experiment data [44–48] in central Au+Au (Pb+Pb) collisions at  $\sqrt{s_{\text{NN}}} = 200$  GeV (2.76 TeV). The solid lines denote predictions from relativistic kinetic equations with the inclusion of the finite sizes of  $d$  and  ${}^3\text{He}$ , and they describe the data very well. We have also studied the case when treating light nuclei as point particles, and the results remain in agreement with experiment data within uncertainties. This is not surprising as the sizes of the produced mat-

ter in these collisions are over 10 fm and are much larger than those of  $d$  and  ${}^3\text{He}$ . Besides, we find the final yields of  $d$  and  ${}^3\text{He}$  are insensitive to their initial values at QGP hadronization, similar to that found in Refs. [17, 20] for the deuteron. The information of initial light nuclei is largely lost during the hadronic evolution which lasts for more than 15 fm/c.

The situation, however, changes dramatically in  $pp$  collisions at  $\sqrt{s_{\text{NN}}} = 7$  TeV as shown in Fig. 3 (d). For the initial  $d$  and  ${}^3\text{He}$  generated from hadronization, there are uncertainties of the canonical effects [59] for  $pp$  collisions, which are absent in large systems. The initial  $d$  and  ${}^3\text{He}$  in central rapidity ranges approximately from  $1.3 \times 10^{-4}$  to  $5.3 \times 10^{-4}$ , and from  $7.3 \times 10^{-8}$  to  $1.3 \times 10^{-6}$ , respectively. The lower values correspond to an aggressive estimation of the canonical effects, while the upper ones are obtained by neglecting the canonical effects. The uncertainty in our theoretical predictions on the  $p_T$  spectra of  $d$  and  ${}^3\text{He}$ , shown in Fig. 3 (d) by the shaded bands, reflects the uncertainty in the initial  $d$  and  ${}^3\text{He}$  yields. For the case of treating light nuclei as point particles, we find the spectra of  $d$  and  ${}^3\text{He}$  are significantly overestimated, regardless of the initial yields of  $d$  and  ${}^3\text{He}$ . After taking into account of their sizes, both spectra are reduced, and they now agree with the experimental data. Unlike in central Au+Au and Pb+Pb collisions, we find the final yields of  $d$  and  ${}^3\text{He}$  in  $pp$  collisions to be sensitive to their initial values after their sizes are taken into account. This is mainly because the reaction rate is not large enough to achieve chemical equilibrium among nucleons, deuterons and helium-3 during the very short collision time of merely a few fm/c. As a result, both the hadronization mechanism and the many-body hadronic reactions play important roles in light (anti-)nuclei production in high-energy  $pp$  collisions. This finding will also be relevant for the indirect search of dark matter from studying light (anti-)nuclei in cosmic rays.

## V. SUMMARY

We have developed a stochastic method to solve the relativistic kinetic equations for light nuclei production from many-body reactions in the hadronic matter produced in high-energy nuclear collisions. With the initial hadron distributions generated from the MUSIC hydrodynamic model or the AMPT model, we have found that the  $d$  and  ${}^3\text{He}$   $p_T$  spectra measured in central Au+Au (Pb+Pb) collisions at  $\sqrt{s_{\text{NN}}} = 200$  GeV (2.76 TeV) and in  $pp$  collisions at 7 TeV are well described by the present approach. In particular, the inclusion of light nuclei sizes, which has been neglected in previous transport studies, is essential for describing their suppressed production in  $pp$  collisions. The present kinetic approach has thus significantly advanced our understanding of light nuclei production in high-energy nuclear collisions. This is different from the usual statistical hadronization model and the nucleon phase-space coalescence model, which correspond to the limits of our dynamic model if the final hadronic matter in high-energy nuclear collisions is a uniform and thermalized system.

The present study can be extended straightforwardly

to investigate the production of other light nuclei like  ${}^4\text{He}$  ( ${}^4\text{Li}$ ),  ${}^3\text{H}$ ,  ${}^4\text{H}$ , and exotic states like  $X(3872)$  [60] and the possible  $\Omega$ -dibaryon [61–63] in various collision systems, such as the  $e\bar{e}$ ,  $pp$ ,  $pA$  and  $AA$  collisions. With the upcoming high-quality data of light nuclei from RHIC and LHC, the present kinetic approach will further help shed light on more fundamental questions in physics, such as cosmic-ray dark matter detection and the QCD phase structure in relativistic heavy-ion collisions.

## ACKNOWLEDGMENTS

*Acknowledgments*—We thank Lie-Wen Chen, Zi-Wei Lin, Feng Li, Zhen Zhang, and Xiao-Jian Du for helpful discussions, and Chen Zhong for setting up and maintaining the GPU server. This work was supported in part by the U.S. Department of Energy under Award No. DE-SC0015266, No. DE-SC0013460, the Welch Foundation under Grant No. A-1358, the National Science Foundation (NSF) under grant number PHY-2012922, National Natural Science Foundation of China under contract No. 11891070 and No. 11890714, and the Guangdong Major Project of Basic and Applied Basic Research No. 2020B0301030008.

- 
- [1] The STAR Collaboration, Observation of an antimatter hypernucleus, *Science* **328**, 58 (2010).
  - [2] The STAR Collaboration, Observation of the antimatter helium-4 nucleus, *Nature* **473**, 353 (2011).
  - [3] The STAR Collaboration, Measurement of the mass difference and the binding energy of the hypertriton and antihypertriton, *Nat. Phys.* **16**, 409 (2020).
  - [4] S. Mrówczyński, Antideuteron production and the size of the interaction zone, *Phys. Lett. B* **248**, 459 (1990).
  - [5] L. Csernai and J. I. Kapusta, Entropy and cluster production in nuclear collisions, *Phys. Rep.* **131**, 223 (1986).
  - [6] K.-J. Sun, L.-W. Chen, C. M. Ko, J. Pu, and Z. Xu, Light nuclei production as a probe of the QCD phase diagram, *Phys. Lett. B* **781**, 499 (2018).
  - [7] K.-J. Sun, F. Li, and C. M. Ko, Effects of QCD critical point on light nuclei production, *Phys. Lett. B* **816**, 136258 (2021).
  - [8] E. Shuryak and J. M. Torres-Rincon, Light-nuclei production and search for the QCD critical point, *Eur. Phys. J. A* **56**, 241 (2020).
  - [9] D. Zhang for the STAR Collaboration, Energy dependence of light nuclei ( $d, t$ ) production at STAR, in *Proceedings of 13th International Conference on Nucleus-Nucleus Collisions* (Journal of the Physical Society of Japan, Saitama, Japan, 2020).
  - [10] K. Blum, K. C. Y. Ng, R. Sato, and M. Takimoto, Cosmic rays, antihelium, and an old navy spotlight, *Phys. Rev. D* **96**, 103021 (2017).
  - [11] A. Kounine and S. Ting on behalf of the AMS Collaboration, The latest results on high energy cosmic rays, in *Proceedings of The 39th International Conference on High Energy Physics — PoS(ICHEP2018)*, Vol. 340 (SISSA Medialab, 2019) p. 732.
  - [12] P. von Doetinchem, K. Perez, T. Aramaki, S. Baker, S. Barwick, R. Bird, M. Boezio, S. E. Boggs, M. Cui, A. Datta, F. Donato, C. Evoli, L. Fabris, L. Fabbietti, E. F. Bueno, N. Fornengo, H. Fuoke, C. Gerity, D. G. Coral, C. Hailey, D. Hooper, M. Kachelriess, M. Korsmeier, M. Kozai, R. Lea, N. Li, A. Lowell, M. Manghisoni, I. V. Moskalenko, R. Munini, M. Naskret, T. Nelson, K. C. Y. Ng, F. Nozzoli, A. Oliva, R. A. Ong, G. Osteria, T. Pierog, V. Poulin, S. Profumo, T. Pöschl, S. Quinn, V. Re, F. Rogers, J. Ryan, N. Saffold, K. Sakai, P. Salati, S. Schael, L. Serksnyte, A. Shukla, A. Stoessl, J. Tjemsland, E. Vannuccini, M. Vecchi, M. W. Winkler, D. Wright, M. Xiao, W. Xu, T. Yoshida, G. Zampa, and P. Zuccon, Cosmic-ray antinuclei as messengers of new physics: status and outlook for the new decade, *J. Cosmol. Astropart. Phys.* **2020**, 035.
  - [13] A. Andronic, P. Braun-Munzinger, K. Redlich, and J. Stachel, Decoding the phase structure of QCD via particle production at high energy, *Nature* **561**, 321 (2018).
  - [14] R. Scheibl and U. Heinz, Coalescence and flow in ultrarelativistic heavy ion collisions, *Phys. Rev. C* **59**, 1585 (1999).
  - [15] F. Bellini, K. Blum, A. P. Kalweit, and M. Puccio, Examination of coalescence as the origin of nuclei in hadronic collisions, *Phys. Rev. C* **103**, 014907 (2021).
  - [16] Particle Data Group, Review of Particle Physics, *Prog. Theor. Exp. Phys.* **2020**, 083C01 (2020).
  - [17] D. Oliinychenko, L.-G. Pang, H. Elfner, and V. Koch, Microscopic study of deuteron production in PbPb collisions at  $\sqrt{s} = 2.76$  TeV via hydrodynamics and a hadronic af-

- terburner, *Phys. Rev. C* **99**, 044907 (2019).
- [18] P. Danielewicz and G. F. Bertsch, Production of deuterons and pions in a transport model of energetic heavy-ion reactions, *Nucl. Phys. A* **533**, 712 (1991).
- [19] Y. Oh and C. M. Ko, Elliptic flow of deuterons in relativistic heavy-ion collisions, *Phys. Rev. C* **76**, 054910 (2007).
- [20] Y. Oh, Z.-W. Lin, and C. M. Ko, Deuteron production and elliptic flow in relativistic heavy ion collisions, *Phys. Rev. C* **80**, 064902 (2009).
- [21] K.-J. Sun, C. M. Ko, and B. Dönigus, Suppression of light nuclei production in collisions of small systems at the Large Hadron Collider, *Phys. Lett. B* **792**, 132 (2019).
- [22] W. Zhao, K.-J. Sun, C. M. Ko, and X. Luo, Multiplicity scaling of light nuclei production in relativistic heavy-ion collisions, arXiv:2105.14204 (2021), arXiv:2105.14204.
- [23] P. Braun-Munzinger, V. Koch, T. Schäfer, and J. Stachel, Properties of hot and dense matter from relativistic heavy ion collisions, *Phys. Rep.* **621**, 76 (2016).
- [24] E. Shuryak and J. M. Torres-Rincon, Baryon clustering at the critical line and near the hypothetical critical point in heavy-ion collisions, *Phys. Rev. C* **100**, 024903 (2019).
- [25] J. Chen, D. Keane, Y.-G. Ma, A. Tang, and Z. Xu, Antinuclei in heavy-ion collisions, *Phys. Rep.* **760**, 1 (2018).
- [26] A. Ono, Dynamics of clusters and fragments in heavy-ion collisions, *Prog. Part. Nucl. Phys.* **105**, 139 (2019).
- [27] B. Dönigus, Selected highlights of the production of light (anti-)(hyper-)nuclei in ultra-relativistic heavy-ion collisions, *Eur. Phys. J. A* **56**, 280 (2020).
- [28] P. Danielewicz, Quantum theory of nonequilibrium processes, I, *Ann. Phys.* **152**, 239 (1984).
- [29] W. Botermans and R. Malfliet, Quantum transport theory of nuclear matter, *Phys. Rep.* **198**, 115 (1990).
- [30] P. Danielewicz and P. Schuck, Formulation of particle correlation and cluster production in heavy-ion-induced reactions, *Phys. Lett. B* **274**, 268 (1992).
- [31] G. F. Chew, The inelastic scattering of high energy neutrons by deuterons according to the impulse approximation, *Phys. Rev.* **80**, 196 (1950).
- [32] L. Grandchamp and R. Rapp, Thermal versus direct  $J/\Psi$  production in ultrarelativistic heavy-ion collisions, *Phys. Lett. B* **523**, 60 (2001).
- [33] R. R. Whitney, J. Källne, J. S. McCarthy, R. C. Minehart, R. L. Boudrie, J. F. Davis, J. B. McClelland, and A. Stetz, Quasi-free scattering of pions on  $^3,^4\text{He}$ , *Nucl. Phys. A* **408**, 417 (1983).
- [34] A. Klein, C. Gysin, R. Henneck, J. Jourdan, M. Pickar, G. R. Plattner, I. Sick, and J. P. Egger,  $\pi$ -Nucleus quasi-free scattering and multistep processes, *Phys. Lett. B* **187**, 253 (1987).
- [35] A. Klein, C. Gysin, R. Henneck, J. Jourdan, M. Pickar, G. R. Plattner, I. Sick, and J. P. Egger, Quasielastic pion scattering on helium-3, *Nucl. Phys. A* **472**, 605 (1987).
- [36] M. A. Khandaker, M. Doss, I. Halpern, T. Murakami, D. W. Storm, D. R. Tiegler, and W. J. Burger, Inclusive inelastic scattering of 96.5-MeV  $\pi^+$  and  $\pi^-$  by the hydrogen and helium isotopes, *Phys. Rev. C* **44**, 24 (1991).
- [37] R. A. Arndt, I. I. Strakovsky, and R. L. Workman, Analysis of  $\pi d$  elastic scattering data to 500 MeV, *Phys. Rev. C* **50**, 1796 (1994).
- [38] M. Yuly, W. Fong, E. R. Kinney, C. J. Maher, J. L. Matthews, T. Soos, J. Vail, M. Y. Wang, S. A. Wood, P. A. M. Gram, G. A. Rebka, Jr., and D. A. Roberts, Pion double charge exchange and inelastic scattering on  $^3\text{He}$ , *Phys. Rev. C* **55**, 1848 (1997).
- [39] R. Bond, P. J. Johansen, S. E. Koonin, and S. Garpman, Break-up densities of nuclear fireballs, *Phys. Lett. B* **71**, 43 (1977).
- [40] C.-Y. Wong, Dynamics of nuclear fluid. VIII. Time-dependent Hartree-Fock approximation from a classical point of view, *Phys. Rev. C* **25**, 1460 (1982).
- [41] Z. Xu and C. Greiner, Thermalization of gluons in ultra-relativistic heavy ion collisions by including three-body interactions in a parton cascade, *Phys. Rev. C* **71**, 064901 (2005).
- [42] R. Wang, Z. Zhang, L.-W. Chen, and Y.-G. Ma, Nuclear collective dynamics in transport model with the lattice Hamiltonian method, *Front. Phys.* **8**, 330 (2020).
- [43] L.-W. Chen, C. M. Ko, and B.-A. Li, Light cluster production in intermediate energy heavy-ion collisions induced by neutron-rich nuclei, *Nucl. Phys. A* **729**, 809 (2003).
- [44] The STAR Collaboration, Identified baryon and meson distributions at large transverse momenta from Au+Au collisions at  $\sqrt{s_{NN}} = 200$  GeV, *Phys. Rev. Lett.* **97**, 152301 (2006).
- [45] The STAR Collaboration, Yields and elliptic flow of  $d(\bar{d})$  and  $^3\text{He}(\bar{^3}\text{He})$  in Au+Au collisions at  $\sqrt{s_{NN}} = 200$  GeV, arXiv:0909.0566 (2009), arXiv:0909.0566.
- [46] ALICE Collaboration, Centrality dependence of  $\pi$ ,  $K$ , and  $p$  production in Pb-Pb collisions at  $\sqrt{s_{NN}} = 2.76$  TeV, *Phys. Rev. C* **88**, 044910 (2013).
- [47] ALICE Collaboration, Production of light nuclei and anti-nuclei in  $pp$  and Pb-Pb collisions at energies available at the CERN Large Hadron Collider, *Phys. Rev. C* **93**, 024917 (2016).
- [48] The STAR Collaboration, Beam energy dependence of (anti-)deuteron production in Au + Au collisions at the BNL Relativistic Heavy Ion Collider, *Phys. Rev. C* **99**, 064905 (2019).
- [49] ALICE Collaboration, Measurement of pion, kaon and proton production in proton-proton collisions at  $\sqrt{s} = 7$  TeV, *Eur. Phys. J. C* **75**, 226 (2015).
- [50] ALICE Collaboration, Production of deuterons, tritons,  $^3\text{He}$  nuclei, and their antinuclei in  $pp$  collisions at  $\sqrt{s} = 0.9, 2.76, \text{ and } 7$  TeV, *Phys. Rev. C* **97**, 024615 (2018).
- [51] J.-F. Paquet, C. Shen, G. S. Denicol, M. Luzum, B. Schenke, S. Jeon, and C. Gale, Production of photons in relativistic heavy-ion collisions, *Phys. Rev. C* **93**, 044906 (2016).
- [52] C. Shen and B. Schenke, Dynamical initial-state model for relativistic heavy-ion collisions, *Phys. Rev. C* **97**, 024907 (2018).
- [53] G. S. Denicol, C. Gale, S. Jeon, A. Monnai, B. Schenke, and C. Shen, Net-baryon diffusion in fluid-dynamic simulations of relativistic heavy-ion collisions, *Phys. Rev. C* **98**, 034916 (2018).
- [54] C. Shen and L. Yan, Recent development of hydrodynamic modeling in heavy-ion collisions, *Nucl. Sci. Tech.* **31**, 122 (2020).
- [55] C. Shen and B. Schenke, Dynamical initialization and hydrodynamic modeling of relativistic heavy-ion collisions, *Nucl. Phys. A* **982**, 411 (2019).
- [56] A. Monnai, B. Schenke, and C. Shen, Equation of state at finite densities for QCD matter in nuclear collisions, *Phys. Rev. C* **100**, 024907 (2019).
- [57] F. Cooper and G. Frye, Single-particle distribution in the hydrodynamic and statistical thermodynamic models of

- multiparticle production, *Phys. Rev. D* **10**, 186 (1974).
- [58] Z.-W. Lin, C. M. Ko, B.-A. Li, B. Zhang, and S. Pal, Multiphase transport model for relativistic heavy ion collisions, *Phys. Rev. C* **72**, 064901 (2005).
- [59] V. Vovchenko, B. Dönigus, and H. Stoecker, Multiplicity dependence of light nuclei production at LHC energies in the canonical statistical model, *Phys. Lett. B* **785**, 171 (2018).
- [60] Belle Collaboration, Observation of a narrow charmoniumlike state in exclusive  $B^\pm \rightarrow K^\pm \pi^+ \pi^- J/\Psi$  decays, *Phys. Rev. Lett.* **91**, 262001 (2003).
- [61] ExHIC Collaboration, Exotic hadrons in heavy ion collisions, *Phys. Rev. C* **84**, 064910 (2011).
- [62] H. Clement, On the history of dibaryons and their final observation, *Prog. Part. Nucl. Phys.* **93**, 195 (2017).
- [63] ExHIC Collaboration, Exotic hadrons from heavy ion collisions, *Prog. Part. Nucl. Phys.* **95**, 279 (2017).